Supplementary Information for

# Self similarities in desalination dynamics and performance using capacitive deionization

Ashwin Ramachandran [a], Ali Hemmatifar [b], Steven A. Hawks [c], Michael Stadermann [c], Juan G. Santiago [b,*]

[a] Department of Aeronautics & Astronautics, Stanford University, Stanford, California 94305, United States

[b] Department of Mechanical Engineering, Stanford University, Stanford, California 94305, United States

[c] Lawrence Livermore National Laboratory, 7000 East Avenue, Livermore, California 94550, United States

* To whom correspondence should be addressed. Tel. 650-736-1283, Fax 650-723-7657, E-mail: juan.santiago@stanford.edu

# Contents

## S1. RC circuit equivalence with the *numerical* dynamic GCS model

We first describe a simple non-linear RC circuit which is mathematically equivalent to the *numerical* model using GCS type electric double layer (EDL) physics as developed in Section 2.1.

We identify and classify the elements of the CDI cell circuit based on Equation (1), as either resistive or capacitive, or arising from a non-zero potential of zero charge. The voltage distribution in the CDI cell circuit is approximated by

$$V_{cell} = IR + 2V_t\left(\Delta\phi_{mtl} + \Delta\phi_d + \Delta\phi_{st}\right) + V_{PZC}\,. \tag{1}$$

The model's CDI cell resistance is an effective system-wide parameter which approximately takes into the account the following: (i) resistance of external wires/leads, current collector material, and contact resistances, denoted by *R*, (ii) ionic resistance in the spacer, and (iii) an effective ionic resistance within the porous electrodes. The latter two resistances are assumed to depend on the ionic concentration, and are represented by the Ohmic mass transport layer voltage difference, $2V_t\Delta\phi_{mtl}$ in Equation (1).

The capacitive part of the circuit is modeled as the Stern and diffuse layers. Together, the capacitive voltage in the circuit is given by

$$V_{cap} = 2V_t\left(\Delta\phi_d + \Delta\phi_{st}\right) \tag{2}$$

We consider the Stern and diffuse layer capacitors as simple series capacitors given by $C_{st}$ and $C_d$, respectively, since they contain the same electronic charge. Thus, we define an equivalent capacitance, $C_{eq}$ for the CDI circuit as

$$\frac{1}{C_{eq}} = \frac{1}{C_d} + \frac{1}{C_{st}} \tag{3}$$

In CDI operation, typically $C_d$ is at least a factor 10 greater than $C_{st}$, so that $C_{st}$ governs the system capacitance. However, the EDL efficiency is governed by the voltage across the diffuse layer capacitor (see Eq. (14)).

Finally, as a simple model for leakage current due to Faradaic charge transfer reactions, we consider a high (albeit non-linear) resistance $R_p$ in parallel with the equivalent capacitor in Equation (3). Hence, Coulombic efficiency approaches unity for $R_p \to \infty$. Of course, an accurate form of $R_p$ depends on the particular model used to account for leakage currents (e.g., Tafel equation, Butler-Volmer equation; see Qu et al. (2016) and Biesheuvel et al. (2011)) and in general can be written as,

$$R_p = \frac{dV_{cap}}{dI_{leak}} \tag{4}$$

where $I_{leak}$ is the leakage current. The individual resistive and capacitive components of the CDI circuit are depicted in Figure S1a, and an equivalent nonlinear RC circuit is shown in Figure S1b. Next, we derive the expressions for equivalent capacitance and resistance as given by the dynamic GCS model (Section 2.1).

From the GCS model, we derive the differential capacitance for the diffuse layer $C_d$ as

$$C_d = \frac{\partial q}{\partial(2V_d)} = \frac{\partial(\sigma Fa/2)}{\partial(2V_d)} = \frac{\lambda_D caF}{2V_t}\cosh\left(\frac{V_d}{2V_t}\right) \tag{5}$$

Further, the Stern capacitance is given by

$$C_{st} = \frac{\partial q}{\partial(2V_{st})} = \frac{\partial(\sigma Fa/2)}{\partial(2V_{st})} = \frac{c_{st}a}{4} \tag{6}$$

Hence the equivalent capacitance from Equation (3) is given by

$$\frac{1}{C_{eq}} = \frac{4}{c_{st}a} + \frac{2V_t}{\lambda_D caF}\operatorname{sech}\left(\frac{V_d}{2V_t}\right) \tag{7}$$

Next, Ohmic resistance of the mass transport layer $R_{mtl}$ is obtained from

$$I = gcA\Delta\phi_{mtl} = \frac{gcAV_{mtl}}{V_t} = \frac{V_{mtl}}{(V_t/gcA)} \triangleq \frac{V_{mtl}}{R_{mtl}} \ . \tag{8}$$

So, the equivalent resistance for the CDI circuit is the sum of the resistance due to the mass transport layers for the two electrodes and the external constant resistance (all connected in series) as

$$R_{eq} = R + 2R_{mtl} = R + \frac{2V_t}{gcA} \ . \tag{9}$$

From Equation (9), in practical operations, $R_{eq}$ is approximately constant in a DSS cycle assuming that the bulk ionic concentration doesn't change significantly (e.g., unless we strongly deplete the bulk volume). Modeling the effective leakage resistance $R_{p,eq}$ is out of the scope of our work. In high Coulombic efficiency operations, we will assume that $R_{p,eq} \to \infty$.

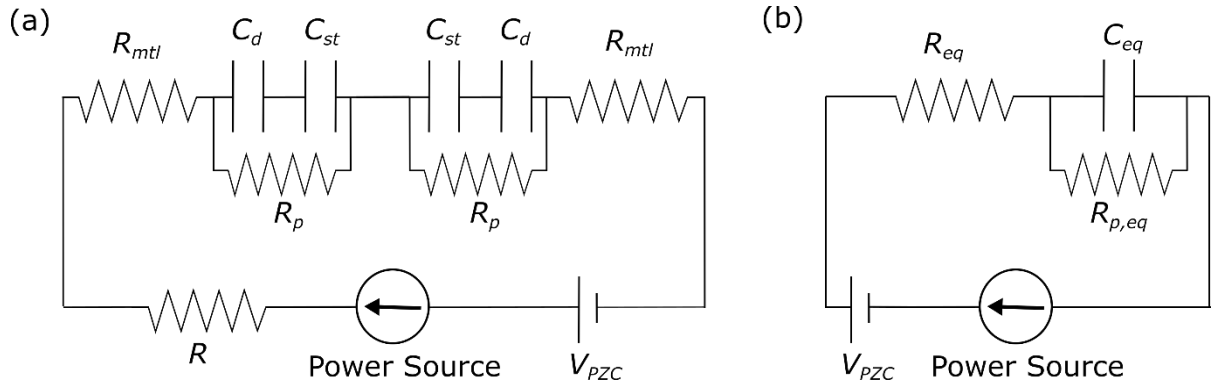


**Figure S1:** (a) Equivalent nonlinear RC circuit equivalent to the GCS model. The capacitive elements are Stern capacitor and $(C_{st})$ diffuse layer capacitor $(C_d)$ connected in series. The resistive components include the external constant resistance $R$ and Ohmic mass transport layer $R_{mtl}$ connected in series, and the leakage resistor $R_p$ in parallel with capacitive elements. The potential of zero charge is represented by a constant voltage source $V_{PZC}$ (b) Equivalent circuit representation of (a) with effective resistances $R_{eq}$ and $R_{p,eq}$, and effective capacitance $C_{eq}$.

Equations (1) through (9) above are mathematically the same as those of Equations (1) to (11) of the main manuscript. We note this equivalent circuit representation (in Fig. S1a) is useful in developing intuition regarding the formulations, but has limited use for closed form solutions. Consider for example the highly non-linear behavior of the diffusive capacitance $C_d$ (Eq. (5) above) or the exponential transition from large to small values for $R_p$ as voltage across the electrodes increases. Nevertheless, the nonlinear RC circuit model (Fig. S1a) is mathematically equivalent to the dynamic GCS model in Section 2.1 and helps identify and study limiting behaviors under which the equivalent circuit (Fig. S1b) can be approximated as a linear RC circuit with an effective resistance and capacitance.

**S2. Derivation of reduced-order formulation with time varying EDL efficiency – the *semi-analytical model***

We here present the derivation of a simplified version of the *numerical* GCS model presented in Section 2.1. As with the simplifications considered here, we assume a constant Stern and equivalent capacitance, and a constant effective resistance for the CDI cell. With these assumptions alone on the *numerical* GCS model, we aim to derive the time dependence of the EDL efficiency during a complete charging and discharging CC cycle under DSS.

First, we denote the electrical charge on the capacitor by $q$ and assume constant current CDI operation ($dq/dt = I$). Now consider a single CC charge and discharge CDI cycle under DSS with current $I$ between cell voltage thresholds $V_{\min}$ and $V_{\max}$. The external voltage at the beginning of the cycle is $V_{\min} + 2IR_{eq}$, where the $2IR_{eq}$ term accounts for the voltage rise above $V_{\min}$ due to current reversal at the beginning of charging (at $t = 0$). So, the voltage distribution in the CDI circuit (as in Figure S1b) is given by

$$V_{\min} + 2IR_{eq} = IR_{eq} + V_{cap}(0) + V_{PZC} \tag{10}$$

Hence, we have the initial voltage on the equivalent capacitor as $V_{cap}(0) = V_{\min} - V_{PZC} + IR_{eq}$. Since the capacitive voltage is distributed between two series capacitors $C_d$ and $C_{st}$ (see Figure S2), we obtain the voltage across the diffuse layer capacitor as

$$V_d(0) = \frac{C_{st}}{C_{st} + C_d}\left(V_{\min} - V_{PZC} + IR_{eq}\right) . \tag{11}$$

Further, the diffuse layer voltage change is given by

$$dV_d = \frac{I\ dt}{C_d} . \tag{12}$$

We then integrate Equation (12) during the charging phase to obtain

$$V_d(t) = \frac{I}{C_d}t + \frac{C_{st}}{C_{st} + C_d}\left[V_{\min} - V_{PZC} + IR_{eq}\right] = \frac{I}{C_d}t + \frac{C_{eq}}{C_d}\left[V_{\min} - V_{PZC} + IR_{eq}\right] \tag{13}$$

Equation (13) shows how our *semi-analytical* approach for the diffuse layer voltage as increasing linearly with time (see Figure S2 for the exact variation from the *numerical* model of Section 2.1). The rate of increase of $V_d$ is governed by the charging current and the diffuse layer capacitance (assumed here to be constant during an operation). Now, we invoke GCS theory to account for the effects of dynamic charge efficiency on salt removal, and obtain an expression for dynamic variation of differential EDL charge efficiency as

$$\lambda_{dl}\left(t\right)=\tanh\left(\frac{V_d}{2V_t}\right)=\tanh\left(\frac{I}{2V_tC_d}t+\frac{C_{eq}}{2V_tC_d}\left[V_{\min}-V_{PZC}+IR_{eq}\right]\right) \tag{14}$$

Equations (13) and (14) are valid for the charging phase of the cycle. For the discharge step with current $-I$ which results in an initial cell voltage at discharge equal to $V_{\max}-2IR_{eq}$, we derive diffuse layer voltage and differential EDL efficiency during discharge as

$$V_d\left(t\right)=-\frac{I}{C_d}t+\frac{C_{eq}}{C_d}\left[V_{\max}-V_{PZC}-IR_{eq}\right] \tag{15}$$

and

$$\lambda_{dl}\left(t\right)=\tanh\left(\frac{-I}{2V_tC_d}t+\frac{C_{eq}}{2V_tC_d}\left[V_{\max}-V_{PZC}-IR_{eq}\right]\right). \tag{16}$$

In this *semi-analytical* model, though the diffuse layer voltage $V_d$ varies linearly with time during the cycle, the differential EDL charge efficiency varies nonlinearly in a hyperbolic tangent form as described by the *numerical* GCS model (Eqn. (14)). Thus, combining Equations (14) and (16) for the differential EDL efficiency variation during charging and charging, along with the mixed reactor model, the desalination dynamics is governed by

$$\frac{d\left(\Delta c\right)}{d(t/\tau)}+\Delta c=\frac{I\lambda_c\lambda_{dl}(t/\tau)}{FQ}\ . \tag{17}$$

The model presented in this section is a reduction from the two coupled ordinary differential equations (ODEs) for effluent concentration and electrical charge of the *numerical* GCS model (c.f. Section 2.1 of main manuscript), to a single ODE for effluent concentration (given by Eqs. (14), (16) and (17)). Although the model described here results in a single ODE for in time (Equation (17)), we cannot find an analytical expression for $\Delta c\left(t\right)$. Equation (17) must be solved numerically and hence, we refer to this reduced order model with time varying EDL efficiency as a *semi-analytical* model.

Below in Figure S3, we benchmark results from the *semi-analytical* model developed in this section to *numerical* GCS model developed in Section 2.1 of the main manuscript for a constant current (CC) operation between cell voltages $V_{\min}$ and $V_{\max}$. We see in Fig. S3 that the *semi-analytical* reduced order model (dashed lines) does indeed capture the time variation in differential EDL charge efficiency and effluent concentration quite accurately when compared with the complete *numerical* GCS model (solid lines). We attribute most of the over-prediction of the analytical model compared to the semi-analytical model due to the analytical model's assumption of a continuous linear increase in the diffuse layer voltage. In the semi-analytical model, the diffuse layer voltage is sub-linear near $V_{\max}$, and thus the semi-analytical model has lower values of EDL efficiency near $V_{\max}$ when compared to the analytical model.

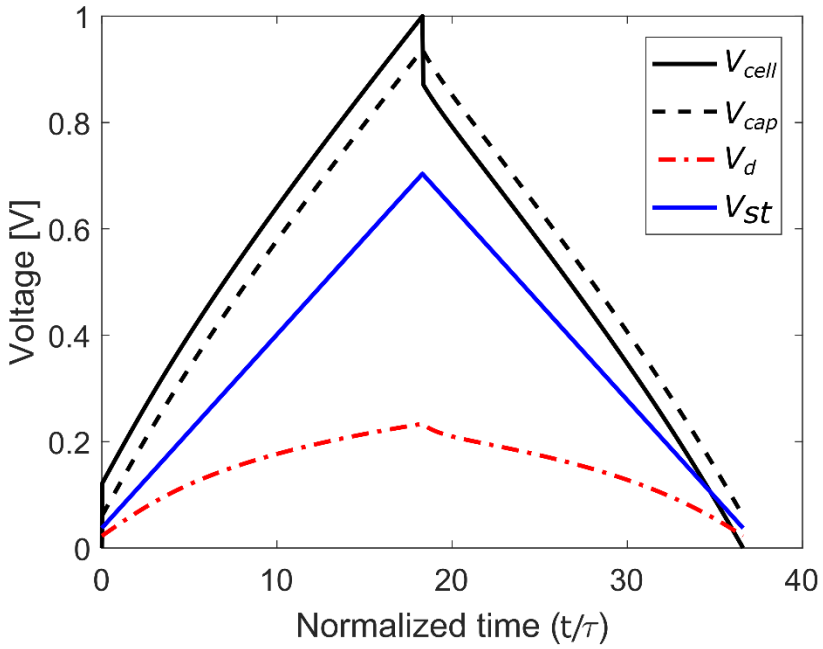


**Figure S2:** Voltage distribution in the capacitive elements of the CDI electrical circuit as predicted by the dynamic GCS model under DSS. Shown are voltage differences across the equivalent capacitor $\left(V_{cap}\right)$, Stern capacitor and $\left(V_{st}\right)$ diffuse layer capacitor $\left(V_d\right)$, and the external cell voltage $\left(V_{cell}\right)$. For the GCS model results shown here, we used $c_{st} = 0.2$ F/m$^2$, $a = 824$ m$^2$, $g = 10$ μm/s, $R = 1$ Ohm, $c_0 = 20$ mM, $A = 125$ cm$^2$, $\forall = 4.5$ ml, $V_{PZC} = 0$ V. and $Q = 9$ ml/min, with no leakage currents. The operation considered here is CC charge discharge with 50 mA between $V_{\min} = 0$ V and $V_{\max} = 1$ V. Note that the external cell voltage and the voltage across the Stern capacitor vary nearly linear with time, and the diffuse layer voltage is only roughly linear. The reduced order models we presented in Section 2.2 of the main manuscript approximate the diffuse layer voltage variation to be linear with time.

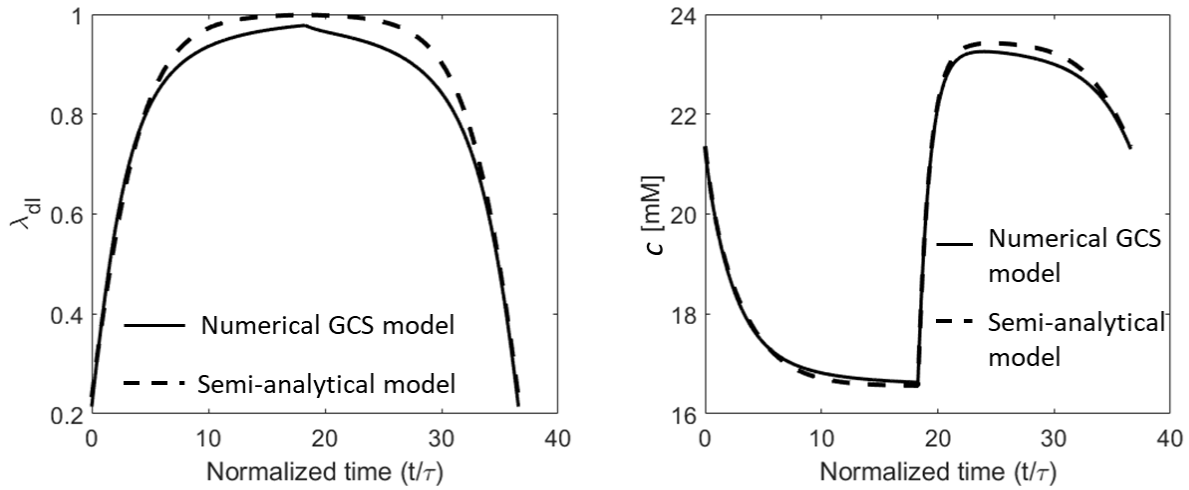


**Figure S3:** Comparisons of time variation of differential EDL efficiency (left), and effluent concentration (right), as predicted by the *numerical* dynamic GCS model (solid lines) (presented in Section 2.1 of the main manuscript) and the reduced order *semi-analytical* model (presented in Section 2.2 of the main manuscript) with time varying EDL efficiency (dashed lines). The reduced order model captures the underlying EDL charging mechanism predicted by the dynamic GCS model quite well. There is a slight over-prediction by the reduced order model in the peak differential EDL efficiency (less than 6% difference) and concentration reduction (less than 2% difference).

Finally, we calculate the average EDL efficiency during a complete cycle by time averaging expressions (14) and (16), to give

$$\bar{\lambda}_{dl}\left(t_{ch}\right)=\left\langle \lambda_{dl}\left(t\right)\right\rangle_{0}^{t_{ch}}=\left\langle \lambda_{dl}\left(t\right)\right\rangle_{t_{ch}}^{t_{disch}}=\frac{\log\left[\cosh\left(\alpha_{\max}\right)\right]-\log\left[\cosh\left(\alpha_{\min}\right)\right]}{\alpha_{\max}-\alpha_{\min}} \tag{18}$$

where, $\alpha_{\min}=\left(1-\frac{C_{eq}}{C_{st}}\right)\left[\frac{V_{\min}-V_{PZC}+IR_{eq}}{2V_t}\right]$ and $\alpha_{\max}=\left(1-\frac{C_{eq}}{C_{st}}\right)\left[\frac{V_{\max}-V_{PZC}-IR_{eq}}{2V_t}\right]$. Note that the average EDL efficiency during charging and discharging in this model are equal, which is consistent with the DSS condition that salt removed during charging is equal to salt regenerated during discharging. Further, note that operationally, the average EDL efficiency is a strong function of the effective voltage thresholds, i.e., $V_{low}=V_{\min}-V_{PZC}+IR_{eq}$ and $V_{high}=V_{\max}-V_{PZC}-IR_{eq}$ as

$$\bar{\lambda}_{dl}=\bar{\lambda}_{dl}\left(V_{low},V_{high}\right)\ . \tag{19}$$

In reality, we note that experimental data suggests that the equivalent capacitance of the CDI cell is a weak function of flow rate, especially at low flow rate values where the effects of diffusion and dispersion are significant. In our study here, we consider operations at sufficiently high flow rates such that the equivalent capacitance is nearly constant. Also, we note that the Stern

capacitance can vary slightly with the amount of EDL charge (see Biesheuvel et al., 2011). In our work, however, we approximate Stern capacitance by a constant value during a specific operation.

## S3. Derivation of reduced-order model dynamics with constant EDL efficiency – an *analytical* model and solution

We here add details of the *analytical* model and solution for effluent concentration that was presented in Section 2.3 of the main manuscript. As a further simplification to the *semi-analytical* model of Sections 2.2 and S2, we assume that the effects of time variation of EDL efficiency as described by Equations (13)-(17) can be represented by using a constant effective value of the EDL efficiency. This effective EDL efficiency value is given by the average value $\bar{\lambda}_{dl}$ that we derived in Equation (18). Thus, for the *analytical* model discussed in this section (and Section 2.3 of the main manuscript), the dynamics equation (17) simplifies to

$$\underbrace{\frac{d(\Delta c)}{dt}+\frac{\Delta c}{\tau}}_{\text{Natural response}}=\underbrace{\frac{I(t)\lambda_c\bar{\lambda}_{dl}}{FQ\tau}}_{\text{Forcing function}}\ , \tag{20}$$

which, as we show below has analytical solutions for certain operations. A similar assumption (i.e. a constant, cycle-averaged value for $\bar{\lambda}_{dl}$) was used by Hawks et al. (2018) to study and highlight the effects of instantaneous flow efficiency.

### *S3.1. Solution for open circuit flush – no forcing, natural response*

For $I(t)=0$ , we obtain the natural response discussed in Section 4.1 of the main manuscript, and the solution of (20) is

$$\Delta c(t)=\Delta c(0)e^{-t/\tau}\ . \tag{21}$$

### *S3.2. Solution for constant current forcing*

When $I(t)=I$ , we obtain the natural response, and the solution of (20) is then

$$\Delta c(t)=\underbrace{\frac{I\bar{\lambda}_{dl}}{FQ}\left(1-e^{-t/\tau}\right)}_{\text{Forced response}}+\underbrace{\Delta c(0)e^{-t/\tau}}_{\text{Natural resposne}}. \tag{22}$$

where $\bar{\lambda}_{dl}$ is given by Equation (18). Note that the natural response decays when DSS is reached, so only the forced response in Equation (22) dominates the long-term dynamics. Hence, for sufficient duration of CDI operation (for times sufficiently longer than ~5 $\tau$ ), the cell performance becomes independent of its initial condition and reaches a dynamic steady state. The cell can be said to "forget" its initial state as it transitions to DSS.

Using the analytical solution in Equation (22), we here briefly describe the procedure to obtain flow efficiency. First, we use periodic conditions for $\Delta c(t)$ at the end of the cycle, i.e., $\Delta c(0) = \Delta c\left(t_{cycle}\right)$ to obtain the initial value of $\Delta c(t)$ at the beginning of a cycle. Further, we evaluate time points corresponding to $\Delta c(t) = 0$ and calculate the salt removed (in moles) at effluent using $\Delta N_{eff} = \int_{t|\Delta c(t)>0} Q\Delta c(t')dt'$ . Finally, we estimate flow efficiency using $\lambda_{fl} = \dfrac{\Delta N_{eff}}{\left(q\bar{\lambda}_{dl}/F\right)}$ , where $q = \int_{\text{charging}} I(t)dt$ .

For the CC operation considered in this work, we derive

$$\Lambda_{cycle} = \frac{\Delta N_{eff}}{It_{ch}} F \approx \bar{\lambda}_{dl}\lambda_c \left( 1 - \frac{2}{\left(\frac{t_{ch}}{\tau}\right)} \log\left[ \frac{2\exp\left(\frac{t_{ch}}{\tau}\right)}{1+\exp\left(\frac{t_{ch}}{\tau}\right)} \right] \right) \triangleq \bar{\lambda}_{dl}\lambda_c\lambda_{fl} . \tag{23}$$

For a more detailed discussion on such a treatment of flow efficiency for CC operation, refer to Hawks et al. (2018).

In Eq. (23), we will use our analytical estimate for $\bar{\lambda}_{dl}$ given by Eq. (18). Also, note that $t_{ch}/\tau$ depends on both $Q/I$ and the voltage window $\Delta V$ (as given by Eq. (19) of the main manuscript), and hence

$$\lambda_{fl} = \lambda_{fl}\left(t_{ch}/\tau\right) = \lambda_{fl}\left(\Delta V, Q/I\right) . \tag{24}$$

Therefore, combining Eqs. (19), (23) and (24), we have

$$\Lambda_{cycle}\left(V_{low}, V_{high}, \frac{Q}{I}\right) \approx \bar{\lambda}_{dl}\left(V_{low}, V_{high}\right)\lambda_{fl}\left(\Delta V, \frac{Q}{I}\right)\lambda_c . \tag{25}$$

We chose not to employ here a detailed model for $\lambda_c$ in order to highlight the identified similarity variables. Our analysis and conclusions assume judicious choice of $V_{\max}$ such that Faraday losses are small (e.g. $\lambda_c$ greater than about 0.9).

## S4. Implications of the *semi-analytical* and *analytical* reduced order models on desalination dynamics and total salt removed

We here compare the dynamics and average amount of desalination predicted by the *semi-analytical* (time varying EDL efficiency) and *analytical* (time-averaged constant EDL efficiency) reduced order models (discussed in Sections S2 and S3). Note that the set of cell parameters, namely $R_{eq}$ , $C_{eq}$, $C_{st}$ and $\forall$, are identical for the two models. For simplicity, in the current

discussion we assume ~ 50% water recovery with continuous flow operation resulting in half of the total cycle time spent in desalination and remainder in regeneration. We also assume close to unity Coulombic efficiency for the CC operation, and thus equal electrical charging and discharging durations (see Equation (26) of main manuscript) in a cycle. We remind the reader that the effluent concentration has a characteristic phase shift (see Eq. (22)) relative to the applied current; however, with our assumptions here, the duration of electrical charging $t_{ch}$, is the approximately the same as the time spent for desalination $t_{desal}$.

*S4.1. Average concentration reduction and total amount of salt removal*

In this subsection, we explore the implications of the *semi-analytical* and *analytical* models on average salt concentration reduction in a cycle. The time-average reduction in salt concentration, $\Delta c_{avg}$ in a desalination cycle is given by

$$Q\Delta c_{avg} = \Delta N_{eff} = \lambda_{fl}\Delta N_{ads} \tag{26}$$

where $\Delta N_{ads}$ is the salt trapped at the electrodes. We can relate $\Delta N_{ads}$ to the dynamic EDL differential charge efficiency as

$$\Delta N_{ads} = \int_{t_{desal}} \frac{\lambda_{dl}}{F}\, dq = \int_{t_{desal}} \frac{I\lambda_{dl}}{F}\, dt \quad . \tag{27}$$

Combining Equations (26) and (27), we obtain

$$\Delta c_{avg} = \frac{I\lambda_{fl}}{QF} \int_{t_{desal}} \lambda_{dl}\, dt = \frac{I\lambda_{fl}}{QF} \bar{\lambda}_{dl} t_{desal}\,. \tag{28}$$

where the second equality in Equation (28) follows from the definition of the time-average EDL efficiency in Equation (18). Note that the first and second equality in Equation (28) respectively estimate $\Delta c_{avg}$ for the *semi-analytical* model with a time-varying EDL efficiency (Section 2.2 of main manuscript); and estimate $\Delta c_{avg}$ for the *analytical* model using a time-average constant EDL efficiency (Section 2.3 of main manuscript). Hence, by formulation of the *semi-analytical* and *analytical* models, we ensure that both the models predict the same average salt concentration reduction $\Delta c_{avg}$.

Further, since $\Delta c_{avg}$ is the same for the *semi-analytical* and *analytical* models, from Equation (26) we ensure that the total amount (in moles) of salt removed $\Delta N_{eff}$ is also the same between the models. Such parity in important in comparisons of any two such models.

*S4.2. Dynamics of desalination cycles*

Here, we study dynamics of effluent concentration variation as predicted by the *semi-analytical* model with a time-varying EDL efficiency (Section 2.2 of main manuscript) and the *analytical*

model with time-average constant EDL efficiency (Section 2.3 of main manuscript), which are respectively given by Equations (17) and (20). In Figure S4, we show a few comparisons of the effluent concentration as predicted by the two models for CC operations with $I$ = 100 mA, maximum cell voltage threshold of $V_{max}$ = 1 V, flow rate of 9 ml/min, and varying minimum voltage threshold $V_{min}$ between 0-0.3 V.

We show in Fig. S4 that for relatively small voltage windows, i.e., $V_{min}$ values greater than about 0.1 V, the dynamics predicted by the *semi-analytical* and *analytical* models are very similar. We attribute this agreement to the fact that such operation implies small variations of the EDL efficiency (e.g. 0.71 to 0.93 for $V_{min}$ = 0.3 V) consistent with small changes in the diffuse layer voltage $\Delta\phi_d$ during the entire DSS cycle. However, for a large voltage window, i.e., near zero $V_{min}$, the dynamics predicted by the *semi-analytical* and *analytical* models show significant differences. We hypothesize that this difference is due to the large variation of EDL efficiency during the CDI cycle (e.g., 0.28 to 0.93 for $V_{min}$ = 0 V), a feature not captured by the analytical model's use of a constant single value $\overline{\lambda}_{dl}$.

In summary, we find that the dynamics predicted by the *semi-analytical* and *analytical* models are very similar for sufficiently small voltage windows (wherein EDL efficiency variations are small), and they can be quite different for large voltage windows (in which EDL efficiency varies significantly). We further note that the *dynamics* predicted by the time varying EDL efficiency model (*semi-analytical*) is more accurate than the constant EDL efficiency (*analytical*) model when compared with experiments; see Figure 3 of the main manuscript. However, as discussed in Section S4.1, the average salt removal, and efficiencies: flow, EDL, and cycle efficiency, predicted by the *semi-analytical* and *analytical* models are the nearly identical.

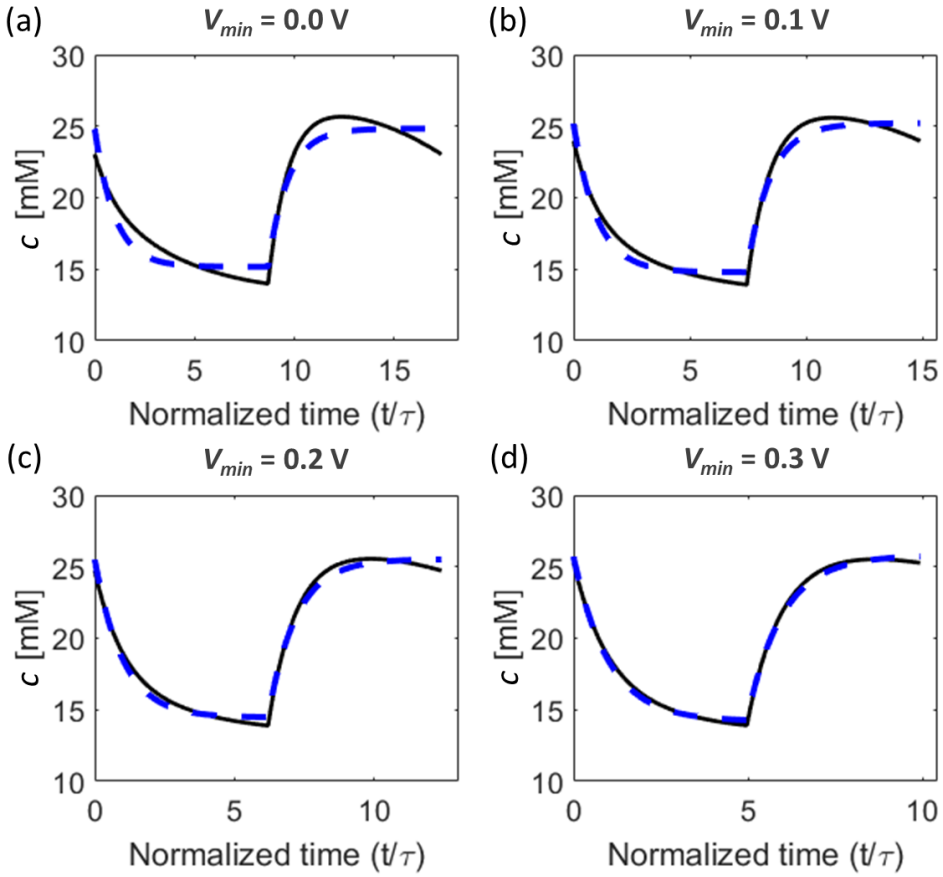


**Figure S4:** Effluent concentration dynamics predicted by the *semi-analytical* model with time varying EDL efficiency (solid lines; c.f. Section 2.2 of main manuscript), and *analytical* model with time-averaged constant EDL efficiency (dashed lines; c.f. Section 2.3 of main manuscript). Results are shown for constant current (CC) operation with $I$ = 100 mA and maximum cell voltage threshold of $V_{max}$ = 1 V, flow rate of 9 ml/min, $V_{PZC} = 0$ V, and varying minimum voltage threshold $V_{min}$. Note that as $V_{min}$ increases, the capacitive voltage and $\Delta\phi_d$ change by smaller amounts. This results in an almost constant EDL efficiency during the cycle and thus a closer agreement between the two models at higher $V_{min}$. We used $C_{eq} = 37.2$ F, $C_{st} = 41.2$ F and $R_{eq} = 1.5$ Ohms for both the models.

*S4.3. Rationale behind choice of reduced order models when comparing with experiments*

As discussed in Sections S4.1, the three efficiencies, namely, average EDL, flow and cycle efficiencies, and $\Delta c_{avg}$ are the same for both *semi-analytical* and *analytical* models. So, for simplicity, we use the *analytical* model in Figs. 4 and 5 of the main manuscript to compare the efficiencies and performance metrics between experiments and model. Note that Productivity and VEC (given in Eqs. (29) and (30) of the main manuscript) are solely dependent on operating conditions, and hence are also the same for the *semi-analytical* and *analytical* models.

In Section S4.2, we showed that the *semi-analytical* model predicts time dynamics of the effluent more accurately compared to the *analytical* model, especially for large voltage windows. Hence, we used the *semi-analytical* model in Fig. 3 of the main manuscript to compare the unique dynamics solution for self-similar operations predicted by the model with experiments.

## S5. Cell Electrochemical Impedance Spectroscopy (EIS) and Cyclic Voltammetry (CV)

We performed a series of preliminary experiments to characterize the CDI cell resistance and capacitance. To characterize resistance, we performed electrochemical impedance spectroscopy (EIS) of the entire assembled cell with 20 mM KCl solution and at flow rate of 6 ml/min. For EIS measurements (see Figure S5), we applied a sinusoidal voltage perturbation with amplitude of 10 mV and scanned over a frequency range from 1 MHz to 10 mHz with 0 V DC bias. We estimate a setup resistance of $R_s \approx 0.92\,\mathrm{Ohm}$ and a contact resistance of $R_{ct} \approx 0.5\ \mathrm{Ohm}$, and a total resistance of $R_{eq} \approx 1.5\ \mathrm{Ohm}$. (see Qu et al., 2016 for a discussion of this parameter extraction).

To estimate cell capacitance, we performed cyclic voltammetry (CV) for the entire cell. For CV, we used a scan rate of 0.2 mV/s, flow rate of 6 ml/min, and 20 mM KCl solution, and performed measurements till a steady state was reached. In Fig. S6, we show the CV measurement for the fifth cycle (under steady state conditions). From the CV data, we estimate an effective cell capacitance of $C_{eq} \approx 38\ \mathrm{F}$.

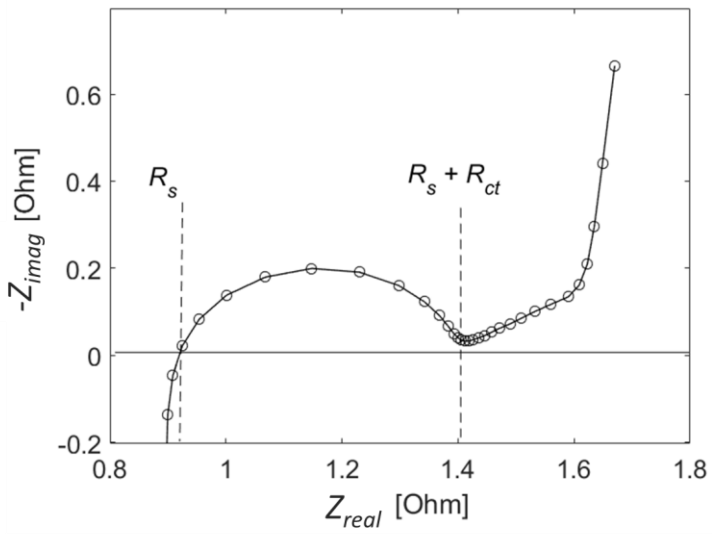


**Figure S5:** Nyquist plot of impedance from electrochemical impedance spectroscopy (EIS) of our fbCDI cell. We applied a sinusoidal voltage perturbation with amplitude of 10 mV and scanned over a frequency range from 1 MHz to 10 mHz with 0 V DC bias. Highlighted are estimates of the

setup resistance ($R_s$) and contact resistance ($R_{ct}$) (see Qu et al., 2016 for a discussion of this parameter extraction).

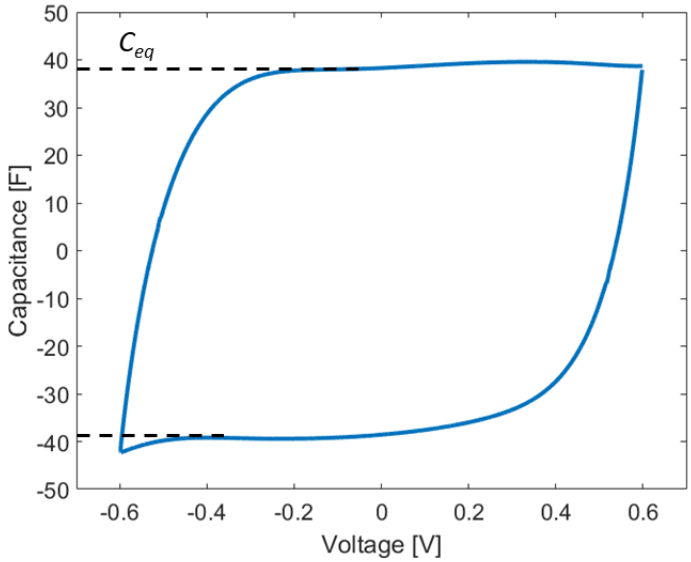


**Figure S6:** Cyclic voltammogram of our fbCDI cell performed at a scan rate of 0.2 mV/s, flow rate of 6 ml/min and with 20 mM KCl solution. Shown are the data for the fifth cycle (under steady state conditions). We estimate an effective cell capacitance of $C_{eq} \approx 38$ F.

## S6. Raw voltage and effluent concentration data model parameters extraction

Here, we present measured voltage and effluent concentration from experiments and discuss the choice of parameters used in the *semi-analytical* and *analytical* reduced order models.

*S6.1. Self-similar dynamics - Measured cell voltage versus time, and efficiency calculations corresponding to effluent concentration data shown in Figure 3 of the main manuscript*

In Figure S7, we show measured voltage vs normalized time $(t/\tau)$ corresponding to the effluent concentration data presented in Figure 3 of the main manuscript. In each subfigure of Figures S7 and 3, we chose operations with the same value of current-to-flowrate $Q/I$, and operated between cell voltage thresholds of $V_{min}$ and $V_{max}$ such that, $V_{low} = V_{\min} - V_{PZC} + IR_{eq}$ and $V_{high} = V_{\max} - V_{PZC} - IR_{eq}$ were the same for each case. Such operation enabled us to study self similarity in effluent dynamics as predicted by both the *semi-analytical* (c.f. Section 2.2) and *analytical* (c.f. Section 2.3) reduced order models. Note that the normalized charging and discharging duration for all cases in each subfigure of Figure S7 are almost equal.

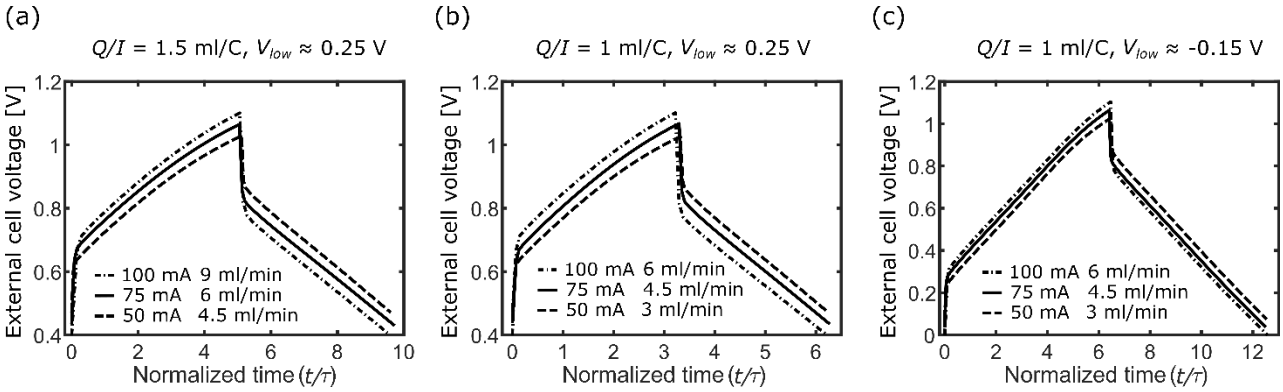


**Figure S7:** Supplement data for Figure 3 of the main manuscript. Measured cell voltage versus normalized time for (a) three cases of $Q/I$ = 1.5 ml/C with current values of 50, 75 and 100 mA, and flow rates of 4.5, 6 and 9 ml/min respectively, between $V_{low}$ = 0.25 V and $V_{high}$ = 0.65 V, (b) three cases of $Q/I$ = 1 ml/C with current values of 50, 75 and 100 mA, and flow rates of 3, 4.5 and 6 ml/min respectively, between $V_{low}$ = 0.25 V and $V_{high}$ = 0.65 V, (c) the same current and flow rates as in (b), but with $V_{low}$ = 0.25 V and $V_{high}$ = 0.65 V (larger voltage window compared to (a) and (b)). Using a value of $C_{eq}$ = 37.2 F and $R_{eq}$ = 1.55 Ohms, the cell voltage windows $V_{\min}$ and $V_{\max}$ were chosen such that $V_{low}\left(=V_{\min}-V_{PZC}+IR_{eq}\right)$ and $V_{high}\left(=V_{\max}-V_{PZC}-IR_{eq}\right)$ are equal in each case. Further, we estimated a value of $C_{st}$ = 41.2 F for the reduced order models that best fit the dynamic data.

Further, in Table S1, we present experimentally determined average EDL efficiency, flow efficiency, cycle efficiencies, average salt reduction, productivity, and volumetric energy cost for the operations presented in Figures 3 and S7. Note that for self-similar operations (grouped together with the same shading) average EDL efficiency, flow efficiency, cycle efficiency, and average salt removal values are nearly the same. However, volumetric energy cost and productivity change across self-similar operations since they depend on flow rate and current explicitly.

**Table S1:** Experimental values of cycle averaged EDL efficiency, cycle averaged flow efficiency, cycle efficiencies, average salt reduction, productivity, and volumetric energy cost for all cases presented in Figures 3 and S7.

| **Operation** | **ΔV** | $\lambda_{dl}$ | $\lambda_{fl}$ | $\Lambda_{cycle}$ | $\Delta c_{avg}$ **[mM]** | **Prod [L/m²/hr]** | **VEC [kWh/m³]** |
|---|---|---|---|---|---|---|---|
| 100 mA, 9 ml/min | 0.25-0.65 V | 0.7 | 0.71 | 0.45 | 3.2 | 21.8 | 0.071 |
| 75 mA, 6 ml/min | 0.25-0.65 V | 0.72 | 0.72 | 0.48 | 3.5 | 16.2 | 0.058 |
| 50 mA, 4.5 ml/min | 0.25-0.65 V | 0.75 | 0.72 | 0.5 | 3.6 | 10.9 | 0.051 |
| 100 mA, 6 ml/min | 0.25-0.65 V | 0.73 | 0.59 | 0.42 | 4.4 | 14.2 | 0.103 |

| | | | | | | | |
|---|---|---|---|---|---|---|---|
| 75 mA, 4.5 ml/min | 0.25-0.65 V | 0.76 | 0.6 | 0.44 | 4.6 | 10.6 | 0.088 |
| 50 mA, 3 ml/min | 0.25-0.65 V | 0.77 | 0.6 | 0.45 | 4.7 | 7.1 | 0.074 |
| 100 mA, 6 ml/min | -0.15-0.65 V | 0.42 | 0.78 | 0.31 | 3.3 | 14.2 | 0.102 |
| 75 mA, 4.5 ml/min | -0.15-0.65 V | 0.41 | 0.78 | 0.31 | 3.3 | 10.6 | 0.081 |
| 50 mA, 3 ml/min | -0.15-0.65 V | 0.4 | 0.78 | 0.3 | 3.2 | 7.2 | 0.064 |

*S6.2. Effect of changing $V_{min}$ on flow, EDL, and cycle efficiencies, and performance metrics: Measured cell voltage and effluent concentration versus time corresponding to data presented in Figures 4 and 5 of the main manuscript*

We show the raw effluent concentration and voltage data from experiments to study the effect of changing $V_{min}$ thresholds (for a fixed $V_{max}$) for CC operation. In Figure S8, we show data for CC operations with $I$ = 100 mA and $I$ = 50 mA, maximum voltage ($V_{max}$) of 1 V, and flow rate of 9 ml/min, for varying minimum voltage $V_{min}$. In Figures 4 and 5 of the main manuscript, we use the raw data shown in Figure S8 to study the effect of changing $V_{min}$ on (i) flow, EDL, and Coulombic efficiencies, and (ii) performance metrics: productivity (Prod), volumetric energy cost (VEC) and average concentration reduction ($\Delta c_{avg}$).

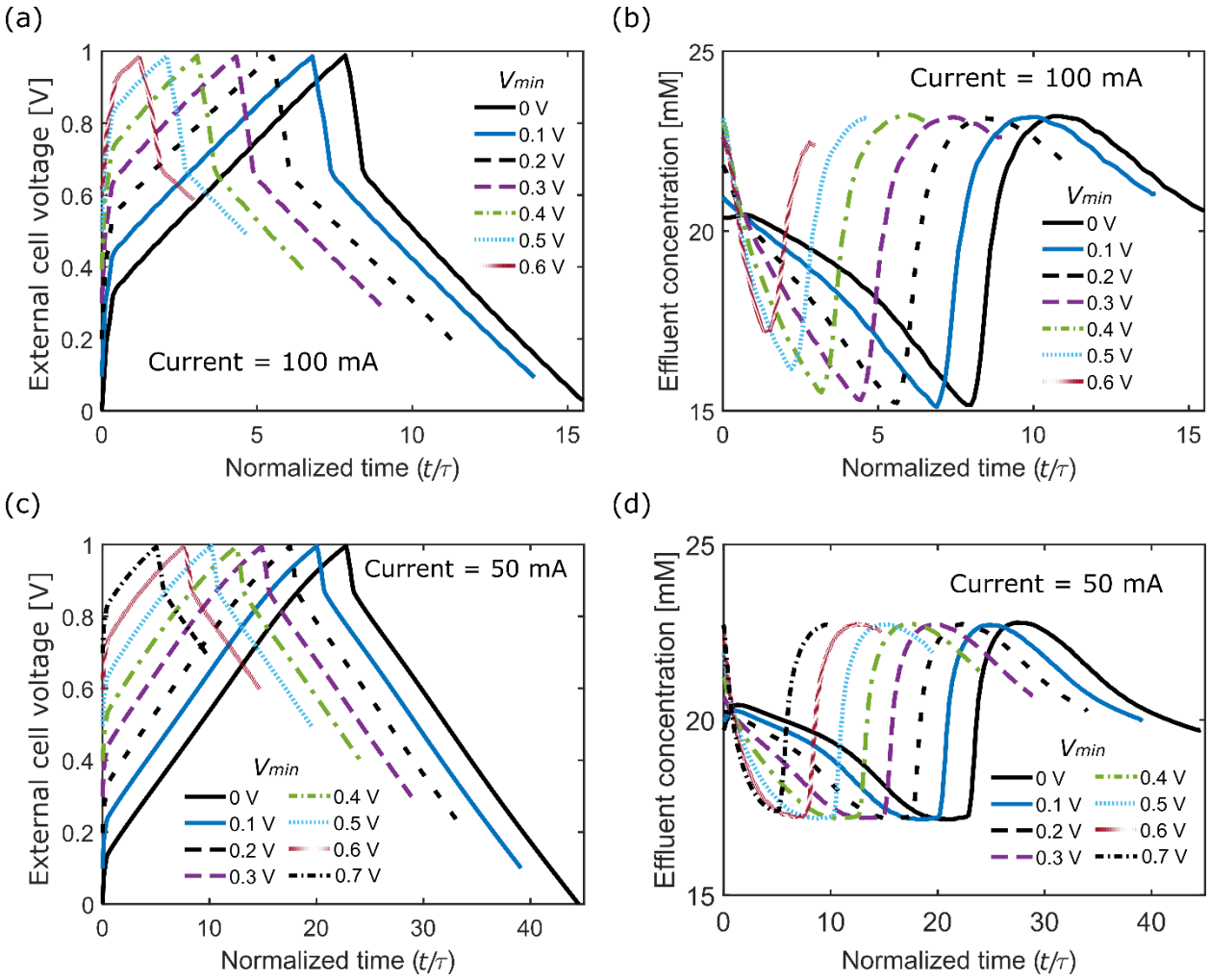


**Figure S8:** Supplement data for Figures 4 and 5 of the main manuscript. Measured values of cell voltage ((a) and (c)) and effluent concentration ((b) and (d)) for a constant current CDI operation with $I$ = 100 mA and $I$ = 50 mA for varying minimum voltage $V_{min}$. The maximum voltage ($V_{\max}$) is 1 V and the flow rate is 9 ml/min. Based on the experiments, we extracted values of $C_{eq}$ = 37.2 F and $R_{eq}$ = 1.55 Ohms, and $C_{st}$ = 41.8 F for 100 mA and $C_{st}$ = 42.8 F for 50 mA cases. Further, ionic repulsion effects were present at low voltages up to 0.3 V, and we accounted for this in our model by subtracting 0.3 V from the cell voltage when comparing model with experiments.

In Table S2, we present Coulombic efficiency values for data presented in Figures 4, 5 and S8. At lower currents, Coulombic losses are higher and show more variation with voltage window (e.g., here at 50 mA, Coulombic efficiency varies between 0.85-0.94). We hypothesize this is because a large duration of the charging and discharging cycle is spent at higher voltages. On the other hand, at higher currents, e.g., 100 mA, Coulombic losses are relatively smaller and show less variation with changing $V_{min}$ (e.g., here at 100 mA, Coulombic efficiency varies between 0.96-0.99)

**Table S2:** Experimentally estimated Coulombic efficiency values for varying minimum voltage ($V_{min}$), for fixed maximum voltage ($V_{max}$) of 1 V, flow rate of 9 ml/min, and currents of 50 mA and 100 mA (same operations as in Figures 4, 5 and S8)

| Current = 50 mA | | | | | | | | |
|---|---|---|---|---|---|---|---|---|
| $V_{min}$ [V] | 0 | 0.1 | 0.2 | 0.3 | 0.4 | 0.5 | 0.6 | 0.7 |
| Coulombic efficiency | 0.94 | 0.93 | 0.91 | 0.9 | 0.88 | 0.87 | 0.86 | 0.85 |

| Current = 100 mA | | | | | | | |
|---|---|---|---|---|---|---|---|
| $V_{min}$ [V] | 0 | 0.1 | 0.2 | 0.3 | 0.4 | 0.5 | 0.6 |
| Coulombic efficiency | 0.96 | 0.99 | 0.98 | 0.97 | 0.98 | 0.96 | 0.96 |

*S6.3. Model parameters extraction*

The equivalent capacitance $C_{eq}$ and resistance $R_{eq}$ were obtained using the voltage-time experimental data values (averaged) as given by

$$C_{eq} = \frac{I}{\left(dV/dt\right)} \tag{29}$$

and,

$$R_{eq} = \frac{|\Delta V|_{I\to -I}}{2I} \ . \tag{30}$$

where $|\Delta V|_{I\to -I}$ is the voltage drop when current reverses sign (with the same magnitude) at the start of discharging. Further we estimated capacitance using Equation (29) during the discharge step as well. In this manner, we obtained $R_{eq}$ = 1.55$\pm$0.28 Ohms and $C_{eq}$ = 37.2$\pm$1.8 F for all our operations, and verified these estimates with EIS and cyclic voltammetry as shown in Figures S5 and S6. Further, for $C_{st}$, we estimated an optimal value that best fitted the dynamic effluent concentration data. For all data presented in this work, we estimated $C_{st}$ = 41.6$\pm$1.3 F. For calculating the residence time $\left(\tau = \forall / Q\right)$ as a function of flow rate $Q$, we used a cell volume of $\forall$ = 4.5 ml (based on Figure 2 of the main manuscript).

*S6.4 Note on modified similarity variable accounting for non-zero potential of zero charge (PZC)*

Experimentally, we observed slight increases in effluent concentration at the beginning of the adsorption phase and this is consistent with ion repulsion effects for $V_{\min} \leq 0.3$ V (e.g., see Fig. S8d). These data imply point of zero potential of approximately ~0.3 V. We hypothesize this is

due to the presence of native surface charges present on the electrode surface. So, for a fair comparison between data and model, we corrected the model by subtracting $V_{PZC} \sim 0.3$ V from the external cell voltage while comparing with experiments, i.e., our similarity variables are $V_{low} = V_{\min} - V_{PZC} + IR_{eq}$ and $V_{high} = V_{\max} - V_{PZC} - IR_{eq}$, where $V_{PZC}$ is the potential of zero charge (equal to 0.3 V for our cell).

In summary, for non-zero $V_{PZC}$, we recommend using similarity variables as: (i) flowrate-to-current ratio $Q/I$, (ii) time normalized by residence time scale, i.e., $t/\tau$, and (iii) modified effective voltage thresholds given by $V_{low} = V_{\min} - V_{PZC} + IR_{eq}$, and $V_{high} = V_{\max} - V_{PZC} - IR_{eq}$.

*S6.5 Previous studies who have identified key variables used in this work*

In our work, we formulated the problem in terms of a set of variables (c.f. Sections 2.2, 2.3 and S6.4) which result in a unique solution for the outflow effluent dynamics. To our knowledge, identification of such a *set* of similarity variables ($Q/I$, $t/\tau$, $V_{low} = V_{\min} - V_{PZC} + IR_{eq}$, and $V_{high} = V_{\max} - V_{PZC} - IR_{eq}$), and identification of such *unique dynamic solutions* (given by the *semi-analytical* and *analytical* models), has not been reported in the past.

We note that subsets of these variables have been explored in CDI. For example, Qu et al. (2018) identified the importance of *Q/I* on the effluent concentration response during charging phase (but not discharge) for a flow through electrode CDI cell, but did not explicitly consider flow efficiency. Also, Johnson and Newman, (1971) and Hawks et al. (2018) identified $t/\tau$ as an important time scale but did not consider effective voltage thresholds. Hawks et al. (2018) further used the residence time scale to estimate flow efficiency for general CC operations, and demonstrated an empirical method to extract effective cell volume for $\tau$. Hemmatifar et al. (2016) identified the importance of a capacitive voltage; that is quantifying cell performance in terms of a modified voltage wherein $IR_{eq}$ is added or subtracted to the external cell voltage for charging and discharging at CC respectively, where $R_{eq}$ was a series resistance. Hemmatifar did not consider effects of flow efficiency or potential of zero charge.

Our work is the first to show that the combination of a set of variables (both cell and operational parameters) together determine a unique effluent dynamic response for CC CDI operation.

**References**


Biesheuvel, P.M., Fu, Y., Bazant, M.Z., 2011. Diffuse charge and Faradaic reactions in porous electrodes. Phys. Rev. E 83, 61507. https://doi.org/10.1103/PhysRevE.83.061507

Biesheuvel, P.M., Zhao, R., Porada, S., van der Wal, A., 2011. Theory of membrane capacitive deionization including the effect of the electrode pore space. J. Colloid Interface Sci. 360, 239–248. https://doi.org/https://doi.org/10.1016/j.jcis.2011.04.049

Hawks, S.A., Knipe, J.M., Campbell, P.G., Loeb, C.K., Hubert, M.A., Santiago, J.G., Stadermann, M., 2018. Quantifying the flow efficiency in constant-current capacitive deionization. Water Res. 129, 327–336. https://doi.org/10.1016/J.WATRES.2017.11.025

Hemmatifar, A., Palko, J.W., Stadermann, M., Santiago, J.G., 2016. Energy breakdown in capacitive deionization. Water Res. 104, 303–311. https://doi.org/10.1016/J.WATRES.2016.08.020

Johnson, A.M., Newman, J., 1971. Desalting by Means of Porous Carbon Electrodes. J. Electrochem. Soc. 118, 510. https://doi.org/10.1149/1.2408094

Qu, Y., Campbell, P.G., Gu, L., Knipe, J.M., Dzenitis, E., Santiago, J.G., Stadermann, M., 2016. Energy consumption analysis of constant voltage and constant current operations in capacitive deionization. Desalination 400, 18–24. https://doi.org/10.1016/j.desal.2016.09.014

Qu, Y., Campbell, P.G., Hemmatifar, A., Knipe, J.M., Loeb, C.K., Reidy, J.J., Hubert, M.A., Stadermann, M., Santiago, J.G., 2018. Charging and Transport Dynamics of a Flow-Through Electrode Capacitive Deionization System. J. Phys. Chem. B acs.jpcb.7b09168. https://doi.org/10.1021/acs.jpcb.7b09168